

Strong-field spatiotemporal ultrafast coherent control in three-level atomsBarry D. Bruner,¹ Haim Suchowski,¹ Nikolay V. Vitanov,^{2,3} and Yaron Silberberg¹¹*Department of Physics of Complex Systems, Weizmann Institute of Science, Rehovot, 76100, Israel*²*Department of Physics, Sofia University, James Bourchier 5 Boulevard, BG-1164 Sofia, Bulgaria*³*Institute of Solid State Physics, Bulgarian Academy of Sciences, Tsarigradsko Chaussée 72, BG-1784 Sofia, Bulgaria*

(Received 3 September 2009; published 10 June 2010)

Simple analytical approaches for implementing strong field coherent control schemes are often elusive due to the complexity of the interaction between the intense excitation field and the system of interest. Here, we demonstrate control over multiphoton excitation in a three-level resonant system using simple, analytically derived ultrafast pulse shapes. We utilize a two-dimensional spatiotemporal control technique, in which temporal focusing produces a spatially dependent quadratic spectral phase, while a second, arbitrary phase parameter is scanned using a pulse shaper. In the current work, we demonstrate weak-to-strong field excitation of ⁸⁵Rb, with a π phase step and the quadratic phase as the chosen control parameters. The intricate dependence of the multilevel dynamics on these parameters is exhibited by mapping the data onto a two-dimensional control landscape. Further insight is gained by simulating the complete landscape using a dressed-state, time-domain model, in which the influence of individual shaping parameters can be extracted using both exact and asymptotic time-domain representations of the dressed-state energies.

DOI: [10.1103/PhysRevA.81.063410](https://doi.org/10.1103/PhysRevA.81.063410)

PACS number(s): 32.80.Qk, 32.80.Xx, 42.50.Hz

I. INTRODUCTION

Progress in the field of coherent control has been closely linked to the development of femtosecond pulse-shaping techniques [1]. Most coherent control schemes have been applied to the weak-field excitation regime, in which the energy level structure of the system is effectively unaltered by the excitation field, and the dynamics can be described using perturbation theory [2,3]. In this regime, coherent control using both adaptive (closed loop) and analytic pulse-shaping schemes have been extensively reported [4–10].

The situation becomes more challenging for high laser intensities when the energy level structure of the system is dressed by the excitation field, and the resulting energy eigenstates and eigenenergies are determined by the time-dependent profile of the ultrafast laser pulse. To date, only a small number of approaches have emerged for identifying pulse-shaping strategies for effective ultrafast strong-field control. Dudovich *et al.* examined a two-level system in cesium atoms and showed that real fields (sine or cosine spectral phases with only one quadrature in the complex plane) could produce light or dark pulses for multiphoton absorption while eliminating power broadening effects [11]. Bayer *et al.* performed selective control of dressed-state populations in potassium using shaped pulses with phase-step height and position as control parameters [12]. Clow *et al.* used an adaptive pulse-shaping loop to optimize a (2 + 1)-photon population transfer in sodium over a large range of laser fluence [13].

In this article, we demonstrate control over multiphoton excitation in a three-level resonant system using simple, analytically derived ultrafast pulse shapes. This approach foregoes the use of adaptive (closed loop) pulse-shaping schemes that employ genetic algorithms to search prohibitively large parameter spaces [14]. The choice of pulse-shaping parameters is based on knowledge of the system Hamiltonian, which can be derived analytically for both weak- and strong-field excitation conditions. The complete dynamics of the

dressed atom can then be solved for any pulse shape that is spanned by the two-dimensional (2D) control space.

II. EXPERIMENT

The layout of the experiment is schematically plotted in Fig. 1(a). Pulses from a 1-kHz Ti:sapphire laser amplifier are shaped with a programmable liquid crystal spatial light modulator (Jenoptik Phase SLM-640) placed in the Fourier plane of a conventional 4-f pulse-shaping configuration. Temporal focusing is employed in order to scan the quadratic phase spatially, mapping the beam's temporal modulation onto different spatial positions in the sample without the need for additional active pulse-shaping elements [15,16]. This not only simplifies the measurement process but also allows for simultaneous scanning of both the quadratic phase (chirp) and a second parameter produced by the pulse shaper. By combining both the spatial and temporal domains of pulse shaping in such a way, this method paves the road toward fast, efficient, and robust creation of multidimensional control landscapes [17].

In the current setup, the temporal focusing configuration consists of a 600 l/mm grating aligned perpendicular to the optical axis of an X10 telescope. The lenses of the telescope are chosen such that the temporally focused beam undergoes minimal spatial focusing in the region of interest in the sample cell, so we require that $z_R \gg L_D$, where z_R is the Rayleigh range for the beam, and L_D is the temporal dispersion length for the applied laser pulse in the sample cell medium. In the experiment, with a π -step phase scanned on the SLM, we can write the complete spectral phase of the pulse with contributions from the SLM and temporal focusing as

$$\tilde{E}(\omega) = \tilde{E}_0 \exp \left[-\frac{(\omega - \omega_1)^2}{\omega_0^2} + i(\phi_{ST} + \phi_{SLM}) \right], \quad (1a)$$

$$\phi_{ST} = \frac{\alpha}{2}(\omega - \omega_1)^2, \quad \phi_{SLM} = \pi\theta((\omega - \omega_1) - \omega_s), \quad (1b)$$

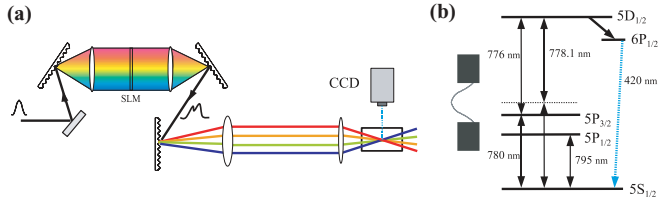


FIG. 1. (Color online) (a) The experimental setup, including the pulse-shaping and temporal focusing components. (b) Energy level structure diagram for multiphoton absorption processes in atomic ^{85}Rb . The excited-state population of the $5D_{1/2}$ level is monitored via fluorescence from the $6P_{1/2}$ level at 420 nm.

where ω_1 corresponds to the central frequency of the laser pulses, ω_0 is the Gaussian half-width of the spectrum, and $\theta((\omega - \omega_1) - \omega_s)$ is the Heaviside step function such that ω_s defines the spectral position of the π -step with respect to ω_1 . The parameter α is the accumulated group delay dispersion (GDD) in the sample, which explicitly depends on the position z along the optical axis [17,18]. We define $z = 0$ to be at the temporal focus of the beam, where the pulse is transform limited in the absence of any additional phase shaping in the SLM. Each element in the SLM is calibrated by applying a π phase to a single pixel, thereby diffracting a portion of the transmitted spectrum out of the beam at a specific wavelength, which was then measured with a sensitive spectrometer (ANDO AQ6315A). In particular, such a calibration provides an unambiguous determination of the absolute phase step position $\omega_1 + \omega_s$, to within the 0.3-nm resolution of the pulse shaper.

In the present experiments, we excite a gas of ^{85}Rb atoms with pulses at a central frequency ω_1 of 778 nm or 2.4 fs^{-1} , corresponding to the two-photon resonance frequency for the $5S_{1/2}$ - $5D_{1/2}$ transition. The spectral width ω_0 is set to 5.5 nm (0.017 fs^{-1}) in order to avoid interaction with the nearby $5S_{1/2}$ - $5P_{3/2}$ resonance at 795 nm. The population in the excited $5D_{1/2}$ level is determined by monitoring the fluorescence at 420 nm from $6P_{1/2}$. To create the 2D plots, we measure the spatially varying fluorescence pattern in the sample for each position of the π -step. The fluorescence is imaged from above using a CCD camera, integrated along the transverse axis, and plotted in a 2D grid as a function of the π -step position and the GDD chirp.

III. RESULTS

Spatiotemporal maps for various laser intensities are shown in Fig. 2. With the π -step located far outside the resonances, excitation occurs only for positive chirp (right-hand side of the images) in both the weak- and intermediate-field regimes. This corresponds to a sequential population transfer via resonant one-photon interactions. As the intensity is increased, the counterintuitive two-photon absorption becomes efficient for negative chirp. With chirped ultrashort pulses, the population transfer process is a variant of the well-known rapid adiabatic passage (RAP) technique [17,19,20]. The excited-state fluorescence was significantly reduced near the zero-GDD axis, where such pulse shapes produce peak intensities high enough to ionize the atom. We note, however, that the three-photon ionization process appears to not be

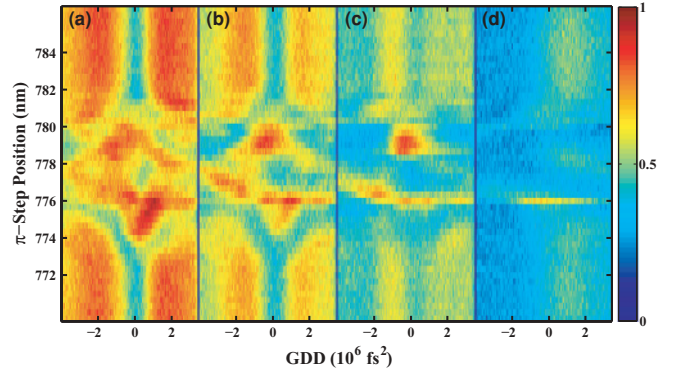


FIG. 2. (Color online) Measured 2D spatiotemporal maps of ^{85}Rb . The spectral position of the π -step and the GDD are plotted along the vertical and horizontal axes, respectively. The peak intensities at zero GDD (zero pulse chirp) are (a) 130, (b) 60, (c) 24, and (d) 10 GW/cm^2 .

avored when the π -step phase is located close to one of the resonant transitions, suggesting quantum interference between the three-photon ionization process and the resonance mediated two-photon process that populates the $5D_{1/2}$ state.

For the weak-field case, with a peak power of $10 \text{ GW}/\text{cm}^2$ at zero GDD [Fig. 2(d)], the π -step induces a population enhancement only when it is located near either of the two resonant transitions at 776 and 780 nm. This enhancement is largely unaffected by the sign or magnitude of the chirp, except for large chirp magnitudes in which the peak intensity is significantly reduced. This result is consistent with earlier studies of resonant multiphoton absorption, in which excitation using transform limited pulses was shown to be less efficient than that with shaped pulses [21]. Additionally, resonant transient enhancement has been demonstrated using chirped pulses [22] and shaped pulses including spectral phase steps [23]. In each of these studies, the dependence of the final population transfer was measured as a function of a single parameter, in part because continuous scans over large ranges of quadratic phase are difficult using compressors and most conventional pulse shapers. Here, we are able to easily map the dependence on both the quadratic phase and π -step control parameters, which becomes crucial as the pulse intensity is increased into the strong-field regime.

For peak intensities larger than $60 \text{ GW}/\text{cm}^2$, the resonant transition features become spectrally broadened, are shifted to bluer regions of the π -step, and their shapes acquire a significant curvature. For $130 \text{ GW}/\text{cm}^2$, as shown in Fig. 2(a), these regions appear as two prominent lobes, with a large enhancement of the overall $5S_{1/2}$ - $5D_{1/2}$ transfer at positive chirp with the π -step located on the $5P_{3/2}$ - $5D_{1/2}$ resonant transition, and at negative chirp with the π -step located on the $5S_{1/2}$ - $5P_{3/2}$ resonance. The curvature of the resonant features indicates that the population transfer process depends sensitively on both control parameters—the π -step position as well as the sign and magnitude of the chirp.

Population transfer in multilevel systems can be easily visualized through the features of the 2D spatiotemporal map. In particular, the data in Fig. 2 are markedly different from

those obtained in a similar weak- to strong-field control study of atomic cesium [17]. The overall dynamics in three-level ^{85}Rb are strongly influenced by the presence of a resonant two-photon absorption pathway, in contrast to the much simpler two-level system in Cs in which the nonresonant two-photon absorption process dominates. The π -step pulse has been shown to be a powerful weak-field control tool when applied to resonant absorption in multilevel systems [23]; however, the dynamics of this interaction have not been substantially explored in the strong-field regime. The detailed features of the control space that emerge in the two-dimensional mappings represent a window into the atomic structure in the presence of strong, shaped laser fields. To decipher the population transfer dynamics, the interdependence of both control parameters must be considered. Unlike in the weak-field limit, in which the probability amplitudes are only dependent on the spectral content and spectral phase of the pulse [24], in the strong-field regime it is also the *temporal shape* and the *temporal chirp* that will determine the dynamics within the time-dependent Schrodinger equation. Hence we must analyze the time dependence of the Rabi frequencies and the detunings.

The three atomic states $|5S_{1/2}\rangle = |1\rangle$, $|5P_{3/2}\rangle = |2\rangle$, and $|5D_{1/2}\rangle = |3\rangle$ are coupled by the strong laser field $E(t) = \frac{1}{\sqrt{2\pi}} \int_{-\infty}^{\infty} \tilde{E}(\omega) e^{-i\omega t} d\omega = \tilde{E}_0 F(t)$, where $\tilde{E}(\omega)$ is the spectral phase (I). In the rotating-wave picture, the laser-excited system is described by the Hamiltonian [25]

$$\mathbf{H}(t) = \begin{bmatrix} \Delta(t) & \frac{1}{2}\Omega_{12}(t) & 0 \\ \frac{1}{2}\Omega_{12}^*(t) & \delta & \frac{1}{2}\Omega_{23}(t) \\ 0 & \frac{1}{2}\Omega_{23}^*(t) & -\Delta(t) \end{bmatrix}, \quad (2)$$

where $\Omega_{ij}(t) = \Omega_0 d_{ij} F(t)$ are the time-dependent Rabi frequencies between states $|i\rangle$ and $|j\rangle$, d_{ij} are the corresponding transition dipole moments (in atomic units), with $d_{12} = 5.87$ a.u. for the $5S_{1/2}$ - $5P_{3/2}$ transition and $d_{23} = 1.77$ a.u. for the $5P_{3/2}$ - $5D_{1/2}$ transition. Ω_0 is the Rabi frequency for a unit dipole moment, and it is conveniently measured in terms of the frequency bandwidth ω_0 . The time-dependent detunings are defined as $\Delta(t) = \partial_t \arg F(t)$, and with ω_{21} defined as the energy difference between the $|1\rangle$ and $|2\rangle$ states, the static detuning is therefore $\delta = \omega_1 - \omega_{21} = 2.15$ nm ($\approx 0.4\omega_0$).

Simulations of the control landscape are presented in Fig. 3. The peak intensities of Fig. 2 correspond (in the absence of chirp and phase step) to peak Rabi frequency units of $\Omega_0/\omega_0 = 5.4, 3.6, 2.3, 1.5$; to obtain the actual peak Rabi frequencies, these values have to be multiplied by the corresponding dipole moment (in a.u.). In the simulation, the second intermediate state $5P_{1/2}$ is also included; because it is off resonance, its contribution has been verified to be minor. Furthermore, an averaging is made over the spatial laser intensity profile (assumed Gaussian) of 15% along one transverse direction and 25% along the other, in order to more closely simulate the experimental conditions. Ionization was estimated to be negligible and was not included in the current simulations.

The effect of the π -step on the atom-field interaction is best understood by considering the asymptotic behavior of the

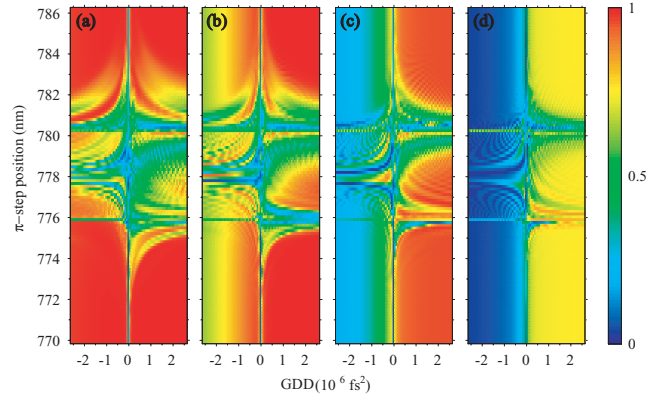


FIG. 3. (Color online) Simulations of 2D spatiotemporal maps for ^{85}Rb . The peak intensities at zero GDD (zero pulse chirp) are (a) 130, (b) 60, (c) 24, and (d) 10 GW/cm^2 .

time-varying part of the electric field $E(t)$. In the limit of large $|t|$, we find

$$F(t) \sim \frac{1}{\sqrt{2(1 - i\alpha\omega_0^2)}} e^{-i\omega_0^2 t^2/4(1 + i\alpha\omega_0^2)} + i\sqrt{\frac{2}{\pi}} e^{-\omega_s^2/\omega_0^2 + i\omega_s(t + \alpha\omega_s)} \left[\frac{1}{t} + O(t^{-2}) \right]. \quad (3)$$

In the absence of a π -step, the second term vanishes and the resulting field is Gaussian-shaped in time and is temporally stretched by a factor of $2(1 + \alpha^2\omega_0^4)^{1/4}$ compared to the transform limited pulse. However, with the π -step, the second term becomes prominent, and the pulse vanishes much more slowly, as $1/t$, with an amplitude proportional to $e^{-\omega_s^2/\omega_0^2}$. In the limit where $t \rightarrow \pm\infty$, this π -step contribution will dominate the intensity envelope of the pulse for any value of the pulse chirp. In this limit, we retrieve the π -step induced detuning at early and late times,

$$\Delta(t) \xrightarrow{t \rightarrow \pm\infty} \omega_s. \quad (4)$$

Thus, the π -step pulse significantly alters the energy level structure of the system and thereby affects the resonant two-photon absorption probability. For remotely positioned phase step ($|\omega_s| \gtrsim \omega_0$, upper and lower parts of the 2D plots), its effect is barely felt by the system, and the dynamics reduce to the process of three-level ladder climbing using only chirped pulses, without a phase step [19]. When the position of the phase step is in the center range of the Fourier spectrum, $|\omega_s| \lesssim \delta$, the proximity of the dressed states to each other leads to increased diabatic exchange of population between them. In particular, the asymptotic behavior of the detuning, as stated in Eq. (4), implies that for large chirp values, choosing either $\omega_s = \pm\delta$ or $\omega_s = 0$ produces an exact degeneracy between a pair of dressed states at early and late times, resulting in considerable mixing between the dressed states. In these regions of the parameter space, the ensuing population splitting leads to greatly reduced transfer and lower observed fluorescence. The dynamics are dramatically changed for smaller pulse chirps, where we note the emergence of regions of high population transfer that can be used for further control strategies in this parameter landscape.

In the strong-field regime, the population dynamics are determined to a large extent by the availability of conditions for adiabatic evolution. The adiabatic states are the time-dependent eigenvectors of the Hamiltonian (2), and the adiabaticity condition requires the suppression of transitions between any pair of adiabatic states $|\varphi_m\rangle$ and $|\varphi_n\rangle$: $|\epsilon_m - \epsilon_n| \gg |\langle \dot{\varphi}_m | \varphi_n \rangle|$, where ϵ_m and ϵ_n are the corresponding energies of these dressed states [26]. The course of the evolution is established by identifying the induced avoided energy level crossings: a wide avoided crossing brings no transition between the dressed states, whereas a narrow avoided crossing implies the system evolves diabatically. For a linearly chirped Gaussian pulse (in the absence of a phase step), the conditions for rapid adiabatic passage in a two-level transition reduce to $\Omega_{\max}^2 \gg |\alpha| \gg \omega_0^2$, which requires large Rabi frequency and large chirp rate [27]. In a chainwise multilevel linkage, such as in the present ladder, it is the *weakest* transition that determines if the evolution is adiabatic. Simple estimates reveal that the stronger transition $5S_{1/2}$ - $5P_{3/2}$ remains adiabatic for the four peak intensities used in the experiment and in the simulations. However, the second transition $5P_{3/2}$ - $5D_{1/2}$ is adiabatic only for intensities 130 and 60 GW/cm², partly adiabatic for 24 GW/cm², and weakly adiabatic for 10 GW/cm². We also point out that for positive chirp rates, the population transfer occurs via consecutive two-level transitions $5S_{1/2} \rightarrow 5P_{3/2} \rightarrow 5D_{1/2}$, whereas for negative chirp rates it occurs via the direct two-photon transition $5S_{1/2} \rightarrow 5D_{1/2}$, which requires higher intensities to saturate and become adiabatic [19]. Thus, in the regions of the 2D parameter space with remotely positioned phase step ($|\omega_s| \gtrsim \omega_0$), the evolution is adiabatic and we find high population in $5D_{1/2}$ for intensities of 130 and 60 GW/cm², except for small chirp rates. For an intensity of 24 GW/cm², high population transfer occurs only for positive chirp rates but only a partial transfer occurs for negative chirp due to insufficient adiabaticity of the two-photon transition $5S_{1/2} \rightarrow 5D_{1/2}$. For intensity 10 GW/cm², partial population transfer occurs for positive chirp, while it is negligibly small

for negative rates. The data from this subset of the 2D map are in excellent agreement with previous observations in ⁸⁵Rb, both by our group [17] and by others [19,20], in which only chirped pulses were used to affect the population transfer.

IV. CONCLUSION

In summary, we demonstrated that strong-field ultrafast excitation in a three-level system can be controlled very efficiently by using a 2D spatiotemporal control scheme. By mapping the data onto a two-dimensional landscape, we analyzed the population transfer dynamics using a time-domain analysis of the interaction between the shaped ultrashort excitation pulses and the ⁸⁵Rb atomic system. The dynamics of the population control were studied using two simple analytically derived control tools—a quadratic phase and a phase step of π —and the concomitant two control parameters: the phase-step position ω_s and the frequency chirp rate α . The phase step in the frequency domain has a dramatic effect in the time domain: it modifies both the amplitude (the Rabi frequency) and the time-dependent frequency of the driving field. It is expected that the speed and simplicity of the spatiotemporal approach will make it possible to push toward more complex control schemes, revealing new information about the dynamics of atoms and providing the ability to coherently control these systems using simple control parameters.

ACKNOWLEDGMENTS

Financial support from the Israel Science Foundation, the Horowitz Foundation, and the European Commission's projects EMALI and FASTQUAST is gratefully acknowledged. B. D. B. acknowledges the Koshland Foundation for financial support. H.S. acknowledges the Azrieli Foundation for financial support. N.V.V. acknowledges financial support from the Bulgarian NSF grants VU-F-205/06 and D002-90/08.

-
- [1] A. M. Weiner, *Rev. Sci. Instrum.* **71**, 1929 (2000).
 [2] M. Shapiro and P. Brumer, *Principles of the Quantum Control of Molecular Processes* (Wiley Interscience, New York, 2003).
 [3] D. J. Tannor, *Introduction to Quantum Mechanics: A Time-Dependent Perspective* (University Science Books, Sausalito, 2006).
 [4] D. Meshulach and Y. Silberberg, *Nature (London)* **396**, 239 (1998).
 [5] D. Oron, N. Dudovich, and Y. Silberberg, *Phys. Rev. Lett.* **89**, 273001 (2002).
 [6] N. Dudovich, D. Oron, and Y. Silberberg, *Nature (London)* **418**, 512 (2002).
 [7] Z. Amitay, A. Gandman, L. Chuntanov, and L. Rybak, *Phys. Rev. Lett.* **100**, 193002 (2008).
 [8] B. Chatel, J. Degert, S. Stock, and B. Girard, *Phys. Rev. A* **68**, 041402 (2003).
 [9] P. Nuernberger *et al.*, *Phys. Chem. Chem. Phys.* **9**, 2470 (2007).
 [10] M. Dantus and V. V. Lozovoy, *Chem. Rev.* **104**, 1813 (2004).
 [11] N. Dudovich, T. Polack, A. Peer, and Y. Silberberg, *Phys. Rev. Lett.* **94**, 083002 (2005).
 [12] T. Bayer, M. Wollenhaupt, C. Sarpe-Tudoran, and T. Baumert, *Phys. Rev. Lett.* **102**, 023004 (2009).
 [13] S. D. Clow, C. Trallero-Herrero, T. Bergeman, and T. Weinacht, *Phys. Rev. Lett.* **100**, 233603 (2008).
 [14] R. S. Judson and H. Rabitz, *Phys. Rev. Lett.* **68**, 1500 (1992).
 [15] H. Suchowski, D. Oron, and Y. Silberberg, *Opt. Commun.* **264**, 482 (2006).
 [16] D. Oron and Y. Silberberg, *Opt. Express* **13**, 9903 (2005).
 [17] H. Suchowski, A. Natan, B. D. Bruner, and Y. Silberberg, *J. Phys. B* **41**, 074008 (2008).
 [18] O. E. Martinez, *IEEE J. Quantum Electron.* **23**, 59 (1987).
 [19] B. Broers, H. B. Van Linden van den Heuvell, and L. D. Noordam, *Phys. Rev. Lett.* **69**, 2062 (1992).
 [20] D. J. Maas, C. W. Rella, P. Antoine, E. S. Toma, and L. D. Noordam, *Phys. Rev. A* **59**, 1374 (1999).
 [21] N. Dudovich, B. Dayan, S. M. Gallagher Faeder, and Y. Silberberg, *Phys. Rev. Lett.* **86**, 47 (2001).

- [22] S. Zamith, J. Degert, S. Stock, B. deBeauvoir, V. Blanchet, M. A. Bouchene, and B. Girard, *Phys. Rev. Lett.* **87**, 033001 (2001).
- [23] N. Dudovich, D. Oron, and Y. Silberberg, *Phys. Rev. Lett.* **88**, 123004 (2002).
- [24] D. Meshulach and Y. Silberberg, *Phys. Rev. A* **60**, 1287 (1999).
- [25] N. V. Vitanov, T. Halfmann, B. W. Shore, and K. Bergmann, *Annu. Rev. Phys. Chem.* **52**, 763 (2001).
- [26] A. Messiah, *Quantum Mechanics* (North-Holland, Amsterdam, 1962).
- [27] G. S. Vasilev and N. V. Vitanov, *J. Chem. Phys.* **123**, 174106 (2005).